

This work was written as part of one of the author's official duties as an Employee of the United States Government and is therefore a work of the United States Government. In accordance with 17 U.S.C. 105, no copyright protection is available for such works under U.S. Law.

Public Domain Mark 1.0

<https://creativecommons.org/publicdomain/mark/1.0/>

Access to this work was provided by the University of Maryland, Baltimore County (UMBC) ScholarWorks@UMBC digital repository on the Maryland Shared Open Access (MD-SOAR) platform.

**Please provide feedback**

Please support the ScholarWorks@UMBC repository by emailing [scholarworks-group@umbc.edu](mailto:scholarworks-group@umbc.edu) and telling us what having access to this work means to you and why it's important to you. Thank you.

# Improved magnetic field generation efficiency and higher temperature spheromak plasmas

To cite this article: R.D. Wood *et al* 2009 *Nucl. Fusion* **49** 025001

View the [article online](#) for updates and enhancements.

## You may also like

- [Effect of geometric and magnetic boundary conditions on magnetic islands in 3D force-free ideal MHD equilibria](#)  
T.E. Benedett and C.J. Hansen
- [Sustained Spheromak Physics Experiment \(SSPX\): design and physics results](#)  
E B Hooper, R H Bulmer, B I Cohen et al.
- [Relativistic Magnetic Explosions](#)  
Maxim V. Barkov, Praveen Sharma, Konstantinos N. Gourgouliatos et al.

# Improved magnetic field generation efficiency and higher temperature spheromak plasmas

R.D. Wood, D.N. Hill, H.S. McLean, E.B. Hooper, B.F. Hudson,  
J.M. Moller and C.A. Romero-Talamás

Lawrence Livermore National Laboratory, Livermore CA 94550, USA

Received 19 September 2008, accepted for publication 1 December 2008

Published 30 December 2008

Online at [stacks.iop.org/NF/49/025001](http://stacks.iop.org/NF/49/025001)

## Abstract

New understanding of the mechanisms governing the observed magnetic field generation limits on the sustained spheromak physics experiment has been obtained. Extending the duration of magnetic helicity injection during the formation of a spheromak and optimizing the ratio of injected current to bias flux produce higher magnetic field plasmas with record spheromak electron temperatures. To explore magnetic field buildup efficiency limits, the confinement region geometry was varied resulting in improved field buildup efficiencies.

**PACS numbers:** 52.55.Ip, 52.35.Py, 52.30.Cv

(Some figures in this article are in colour only in the electronic version)

## 1. Introduction

In this paper we show that, although helicity balance is an important paradigm describing the structure and generation of spheromak magnetic fields, the confinement region geometry, coaxial injector ('gun') current and pulse length also play a significant role in magnetic field buildup efficiency. By extending the helicity injection time during spheromak formation and avoiding overdrive of the gun and the  $n = 1$  central column kink mode by proper matching of gun current and flux, the sustained spheromak physics experiment (SSPX) [1] produces plasmas with peak toroidal fields  $> 1$  T and the highest reported electron temperatures ( $T_e > 500$  eV) for a spheromak plasma, exceeding the temperature previously achieved in the compact torus experiment, CTX [2, 3]. Overdrive of the dc coaxial injector in SSPX during spheromak formation significantly reduces the efficiency of field generation, here defined as  $B_p/I_{\text{gun}}$ , where  $B_p$  is the poloidal magnetic field at the spheromak flux conserver and  $I_{\text{gun}}$  is the gun current. By overdrive, we mean that the current density of the spheromak central column inside the flux conserver exceeds the calculated kink-stability threshold by a wide margin, a condition commonly obtained in previous spheromak experiments [4–7]. This hypothesis is consistent with results of extending the central column in SSPX by lengthening the spheromak confinement region; thus, the overall geometry of the flux conserver must be taken into account when predicting the spheromak fields obtainable by coaxial dc helicity injection.

The physical processes that govern magnetic field generation in magnetized-gun-driven spheromaks [8, 9] will determine the viability of the spheromak as a fusion reactor [10]. These 'magnetically self-organizing' processes also have a broad application to other fusion devices such as the reversed field pinch (RFP) [11] as well as astrophysical and solar phenomena [12]. The SSPX was designed and built to explore the processes that govern magnetic field generation and energy confinement in a spheromak via coaxial helicity injection. Magnetic helicity is a measure of the topological linkage of magnetic flux,  $K = \int_V \mathbf{A} \cdot \mathbf{B} dV$ , (where  $\mathbf{A}$  is the magnetic vector potential). For the gun driven spheromak, magnetic helicity is injected into a flux conserving shell where reconnection reorganizes the magnetic field into an axisymmetric toroidal geometry, dissipating excess energy but approximately conserving helicity in the flux conserver. It follows [11] that Ohmic dissipation is solely responsible for the loss of helicity and thus, during helicity injection, the spheromak magnetic energy should continue to build until Ohmic dissipation matches the available gun power.

In previous experiments using coaxial helicity injection [4–7], spheromak plasmas formed when the applied gun current exceeded a threshold for the ejection of the initial gun bias flux into the flux conserver by a large margin. The gun bias magnetic field in these experiments was mostly radial and confined to the gun region. The threshold condition is reached when the  $\mathbf{J} \times \mathbf{B}$  force due to current flow in the gun overcomes the restoring force of bending field lines in

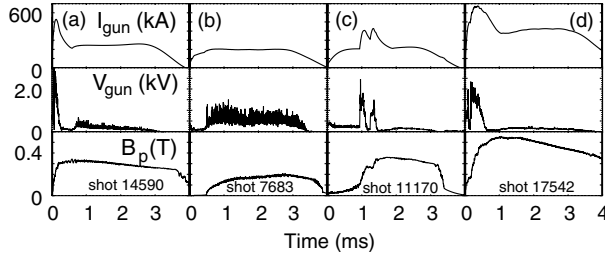


**Figure 1.** Time history of gun current ( $I_{\text{gun}}$ ), gun voltage ( $V_{\text{gun}}$ ) and edge poloidal field for (a) standard formation followed by sustainment, (b) slowly building, (c) double pulse and (d) extended formation discharges.

the gun. For the case of a coaxial gap spanned by a radial magnetic field with total flux  $\psi_{\text{gun}}$ , the normalized gun current  $\lambda_{\text{gun}} = \mu_0 I_{\text{gun}} / \psi_{\text{gun}}$  at the ejection threshold is  $\lambda_{\text{thres}} \approx \pi / \Delta$ , where  $\Delta$  is the cathode–anode gap in the gun region and for the SSPX geometry  $\pi / \Delta = 20 \text{ m}^{-1}$ . The unique gun magnet set in SSPX permits flexible control of the gun bias flux [13, 14]. While SSPX can operate with the ‘standard flux’ condition (i.e. the mostly radial bias field condition described above), greater operational flexibility is achieved using a ‘modified flux’ condition including cases in which a large fraction of the gun flux emerges from near the end of the cathode and gun exit region reducing the ejection threshold considerably. As a consequence, a wide range of ejection thresholds and gun current-to-flux ratios ( $\lambda_{\text{gun}}$ ) is available to explore magnetic field buildup during spheromak formation; for this work all data were obtained using the ‘modified flux configuration’ explained more fully in [14].

## 2. Spheromak formation and magnetic field generation

The recently upgraded SSPX power system [15] is capable of delivering a wide variety of current waveform pulses, which is instrumental in exploring the relationship between the injected gun current and magnetic field buildup. Shown in figure 1 are two previously reported operational modes [16, 17] that demonstrated more efficient field buildup over that observed with a short formation pulse followed by a longer sustainment pulse (figure 1(a)). The first such operating mode (figure 1(b)) did not rely on an initial short (150  $\mu\text{s}$ ) high-current formation pulse, but instead used only a slowly rising ( $\sim 500 \mu\text{s}$ ) current pulse with a 3 ms flat-top current waveform. These slow-start discharges exhibited steadily building helicity content for the duration of the current pulse. For the second mode, double pulse buildup (figure 1(c)), two high-current pulses separated by  $\sim 300 \mu\text{s}$  were added into an existing slow-start discharge leading to a stepwise increase in the spheromak helicity content. While exploring the double pulse operation, a third operating mode was developed by timing the two high-current pulses to provide a single extended formation pulse (figure 1(d)) followed by a sustainment pulse.

Extended formation operation produces higher peak edge poloidal field,  $B_p$ , for a given peak gun current,  $I_{\text{gun}}$ , compared with the other operating modes in SSPX, as shown in figure 2. We use peak  $B_p$  divided by peak  $I_{\text{gun}}$  to define field generation

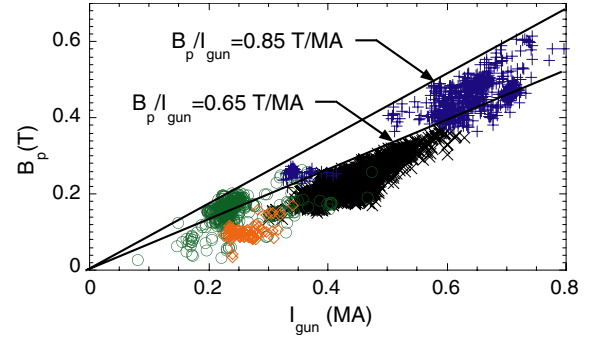


**Figure 2.** Peak edge poloidal field versus peak gun current for standard formation (black x's), slowly building (green circles), double pulse (orange diamonds) and extended formation (blue crosses) discharges.

efficiency rather than energy efficiency,  $\int B^2 dV / 2\mu_0$  divided by  $\int I_{\text{gun}} V_{\text{gun}} dt$ , because peak  $I_{\text{gun}}$  is an important design parameter for spheromak experiments and the latter calculation depends on the pulse shape and time of measurement. For the standard formation (black x's) and double pulse discharges (orange diamonds), there is an upper bound on the maximum edge poloidal field for a given gun current of  $B_p / I_{\text{gun}} = 0.65 \text{ T MA}^{-1}$ . The slowly building (green circles) and extended formation discharges (blue crosses) all have a limit to edge poloidal field of  $B_p / I_{\text{gun}} = 0.85 \text{ T MA}^{-1}$ . Also shown in figure 2, the highest measured edge poloidal field (0.6 T) is obtained with the extended formation current pulse.

Because the extended formation discharges produced the highest edge poloidal fields most efficiently, which in turn leads to higher spheromak electron temperatures, we made a detailed scan of the gun input parameters in order to more fully explore the processes that govern field generation. Due to the finite time required for injected toroidal flux from the gun to convert to poloidal flux in the spheromak [18], the time at which the magnetic field peaks is delayed  $\sim 200\text{--}300 \mu\text{s}$  after the peak in injected current. To explore field buildup we varied the gun current to bias flux ratio. Figure 3 is a plot of the peak buildup efficiency during the formation as a function of  $\lambda_{\text{gun}}$  for extended (blue x's) and standard formation discharges (black x's). As seen in figure 3, standard formation discharges have a modest range of  $\lambda_{\text{gun}}$  that produce similar peak field buildup efficiencies. For extended formation discharges the highest field buildup efficiencies were obtained with increased gun flux ( $\psi_{\text{gun}} \geq 66 \text{ mWb}$ ), which gives gun current-to-flux ratios of  $\lambda_{\text{gun}} \sim 13 \text{ m}^{-1}$ . The extended formation discharges inject helicity longer than standard formation, which produce discharges with higher edge  $B_p$  for a similar peak gun current; however, the range in  $\lambda_{\text{gun}}$  is quite narrow (see figure 3) for extended formation discharges compared with standard formation discharges.

## 3. Current column kink instability analysis

It is useful to consider the basis for the narrow operating range of the extended formation discharges using a model of the kink instability similar to that described in the analysis of the finite length screw pinch [19]. In SSPX with the modified flux configuration, a large fraction of the gun flux

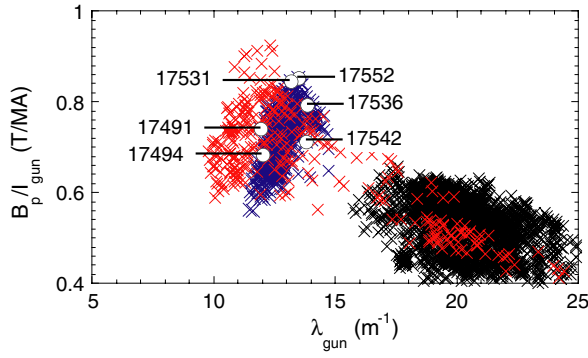


**Figure 3.** Peak edge poloidal field buildup efficiency ( $B_p/I_{\text{gun}}$ ) versus  $\lambda_{\text{gun}}$  for standard formation (black), extended formation (blue) and extended formation with extended flux conserver (red) discharges. Time histories of shots with white circles are in figure 4.

emerges from near the end of the cathode; thus current flows from the bottom of the gun inner electrode to the bottom of the flux conserver forming a cylindrical current carrying plasma column ( $I_{\text{col}}$ ). This cylindrical plasma column is immersed in an axial magnetic field and can be treated as a finite length screw pinch that becomes kink unstable when the column safety factor  $q < 1$ . In previous experiments [6, 20], the observed instability threshold is close to the ‘Kruskal–Shafranov current’ [21, 22],  $I_{\text{ks}} = 4(\pi a)^2 B_z / (\mu_0 L)$  or  $\lambda_{\text{crit}} = \mu_0 I_{\text{crit}} / \psi_{\text{col}} = 4\pi / L$ , with  $a$  the radius of the column,  $B_z$  the current column axial field and  $L$  the cathode-to-bottom-flux-conserver length;  $L = 0.5$  m for SSPX. It is understood that the  $n = 1$  kinked distortion of the current column couples current into the spheromak [23]. Hsu and Bellan [24] also observed this instability in a free-standing current column without a flux conserver in which they measured the current and column length at which the instability occurred.

In SSPX, the gun configuration is such that the plasma column is only line-tied at one electrode; we thus compare our results with a more appropriate [19] 1/2-wavelength instability boundary condition  $\lambda_{\text{crit}} = 2\pi / L$  during spheromak formation, yielding  $\lambda_{\text{crit}} \sim 12.7 \text{ m}^{-1}$ . As seen in figure 3 (blue x’s), most of the extended formation discharges with high ratios of  $B_p/I_{\text{gun}}$  are in a region with  $\lambda_{\text{gun}} \sim 13 \text{ m}^{-1}$  ( $\sim \lambda_{\text{crit}}$ ). Although the field buildup for  $\lambda_{\text{gun}} < 13\text{--}14 \text{ m}^{-1}$  is well described by resistive MHD simulations [25], at higher  $\lambda_{\text{gun}}$  the experimental data fall below the simulations. At lower  $\lambda_{\text{gun}}$  the current column kink and the dynamo action associated with current transport are reduced below that at  $\lambda_{\text{gun}} \sim 13 \text{ m}^{-1}$ , resulting in less energy available to build field. At higher  $\lambda_{\text{gun}}$  the kink is driven more strongly leading to an increase in the amplitude of the  $n = 1$  mode.

For SSPX discharges, the amplitude of the  $n = 1$  mode is calculated by Fourier mode analysis of magnetic probe data. Time histories of similar discharges for the six shots shown in figure 3 (white circles) are compared in figure 4. As shown, the amplitude of the  $n = 1$  mode is increased for discharges with  $\lambda_{\text{gun}} > 13 \text{ m}^{-1}$  ( $I_{\text{gun}} > I_{\text{crit}}$ ) as compared with the discharges with  $\lambda_{\text{gun}} \sim 13 \text{ m}^{-1}$  ( $I_{\text{gun}} = I_{\text{crit}}$ ). Similarly, for discharges with  $\lambda_{\text{gun}} < 13 \text{ m}^{-1}$  ( $I_{\text{gun}} < I_{\text{crit}}$ ) the amplitude of the  $n = 1$  mode is reduced as compared with the discharges with  $\lambda_{\text{gun}} \sim 13 \text{ m}^{-1}$  which results in reduced field buildup efficiency. For discharges with  $\lambda_{\text{gun}} > 13 \text{ m}^{-1}$  the large-amplitude kink may

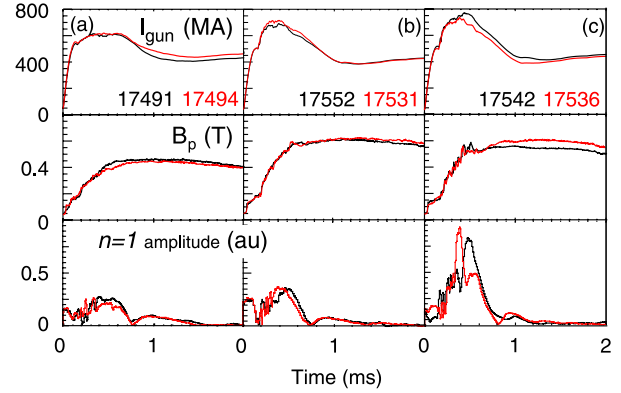


**Figure 4.** Time histories of gun current ( $I_{\text{gun}}$ ), edge poloidal field ( $B_p$ ) and  $n = 1$  mode amplitude for discharges with (a)  $I_{\text{gun}} < I_{\text{crit}}$ , (b)  $I_{\text{gun}} = I_{\text{crit}}$  and (c)  $I_{\text{gun}} > I_{\text{crit}}$ .

significantly distort the instantaneous magnetic geometry of the spheromak. Although the detailed mechanisms leading to the reduction in the rate of field buildup are not clear, this strong distortion will significantly affect magnetic field line trajectories, increasing their deviation from the mean-field geometry. Furthermore, the plasma is likely to have increased contact with the flux conserver wall thereby increasing energy transport leading to increased plasma dissipation.

In SSPX the central column current ( $I_{\text{col}}$ ), column radius ( $a$ ) and field ( $B_z$ ) are not directly measured. Instead, we use the CORSICA MHD reconstruction code [1] to relate the measured edge  $B_p$  to the central column axial field. These reconstructions yield  $B_z \sim 2.6 B_p$  with a central column radius of  $a = 0.12$  m that remains fairly constant for  $\lambda_{\text{gun}}$  between 12 and  $14 \text{ m}^{-1}$  (in agreement with the radius inferred from high-speed camera images [26]). Rearranging the Kruskal–Shafranov threshold equation, the ratio of axial field to current in the central column can be determined using  $B_z I_{\text{ks}} = \mu_0 L / (\pi a)^2$ . Substituting  $B_z = 2.6 B_p$  and assuming all the initial gun current flows from the cathode through the central plasma column (i.e.  $I_{\text{col}} = I_{\text{gun}}$ ), we calculate an edge field to gun current ratio of  $B_p/I_{\text{gun}} \sim 0.9 \text{ TMA}^{-1}$ . As seen in figures 2 and 3, for extended formation discharges (blue crosses), the maximum edge poloidal field buildup efficiency  $B_p/I_{\text{gun}} \sim 0.85 \text{ TMA}^{-1}$  is similar to the Kruskal–Shafranov threshold current ratio.

#### 4. Improved field buildup efficiency

To further test the applicability of the Kruskal–Shafranov current threshold to the SSPX current column during spheromak formation, the length of the flux conserving shell was extended by 20% (10 cm) while keeping the flux conserver radius ( $R$ ) constant. A 20% increase in the flux conserver length,  $L$ , should lead to a 20% increase in field buildup efficiency at 20% lower  $\lambda_{\text{crit}} = 2\pi / L$ . Resistive MHD simulations using NIMROD for the extended flux conserver yielded a similar increase in field buildup efficiency at lower  $\lambda_{\text{gun}}$  [25]. To increase the flux conserver length, the 5 cm long posts that separate the two halves of the flux conserver were replaced with 15 cm long posts; splitting the flux conserver into half allows for diagnostic access at the spheromak midplane.



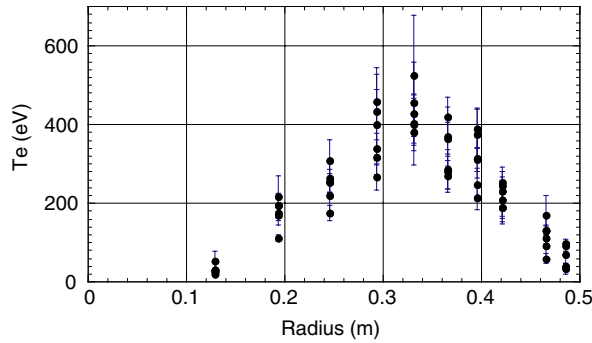


**Figure 5.** Spatial profiles of  $T_e$  for six high-performance extended formation discharges showing measured peak temperature is on (or very near) the magnetic axis.

Results from operations with the extended flux conserver are shown in figure 3 (red x's). As predicted, with the extended flux conserver, the operating range for high edge  $B_p$  shifted from  $\lambda \sim 13$  to  $\lambda \sim 11 \text{ m}^{-1}$  ( $\sim 20\%$ ) and  $B_p/I_{\text{gun}}$ , increased  $\sim 11\%$  from  $\sim 0.85$  to  $\sim 0.95 \text{ TMA}^{-1}$ . The observed field buildup efficiency ( $0.95 \text{ TMA}^{-1}$ ) is less than predicted because the increased flux conserver gap allowed plasma to escape the confinement region thus lowering the field buildup efficiency. Ideally, the flux conserver would have been extended using a ring, but the impending shutdown of the experiment did not allow sufficient time for this. Because of the extended gap in the solid wall, the spheromak boundary extended into the diagnostic gap and the posts acted as limiters, as verified by damage to their plasma-facing surfaces. We would expect that further increasing the flux conserver length should lead to increased field buildup efficiency at lower  $\lambda_{\text{gun}}$  until the flux conserver length-to-radius ratio  $L/R \sim 1.6$ , at which point the spheromak equilibrium becomes tilt unstable [27].

## 5. High electron temperature results and summary

As a result of extending the formation pulse and operating at the optimum  $\lambda_{\text{gun}} \sim \lambda_{\text{crit}} \sim 13 \text{ m}^{-1}$  in SSPX to produce higher magnetic fields, we have achieved record peak electron temperatures in a spheromak ( $T_{e0} > 500 \text{ eV}$ ). Comparing the gun voltage traces for an extended formation discharge (figure 1(d), shot 17542, peak  $T_e = 460 \text{ eV}$ ) and a standard formation (figure 1(a), shot 14590, peak  $T_e = 350 \text{ eV}$ ) discharge shows that the helicity injection time during formation (first  $600 \mu\text{s}$ ) is extended by a factor of 3 over the standard formation discharge shown in figure 1(a), which in turn extends the field buildup time leading to higher edge poloidal field. Since most SSPX temperature data are bounded by an electron  $\beta_e \sim 5\%$  [14], an increase in temperature is obtained by increasing the magnetic field strength ( $T_e \sim \beta B^2$ ) while maintaining a nearly constant electron density ( $n_e \sim 1 \times 10^{14} \text{ cm}^{-3}$  for typical SSPX discharges). Spatial profiles (10 radial positions) of the electron temperature for six high-performance extended formation discharges are shown in figure 5.

In summary, extending the duration of magnetic helicity injection during spheromak formation while operating close to the Kruskal–Shafranov threshold current for a single-ended column produces spheromak discharges with higher magnetic fields more efficiently than does using shorter injection pulses driven at much higher relative currents. Although helicity balance is an important paradigm describing the structure and generation of spheromak magnetic fields, we show that the confinement region geometry plays a significant role in field buildup efficiency through the Kruskal–Shafranov stability condition, suggesting that lengthening the current column, which forms during the formation of the spheromak, should lead to increased field buildup efficiency. As predicted, extending the flux conserver length generated spheromaks with increased field buildup efficiency.

## Acknowledgments

The authors gratefully acknowledge D.D. Ryutov, B.I. Cohen, T.K. Fowler and L.L. Lodestro and thank R.W. Geer, R.O. Kempton and S.R. Gordon for machine and diagnostic operation. This work was performed under the auspices of the US Department of Energy by Lawrence Livermore National Laboratory under Contract DE-AC52-07NA27344.

## References

- [1] Hooper E.B. *et al* 1999 *Nucl. Fusion* **39** 863
- [2] Jarboe T.R. *et al* 1983 *Phys. Rev. Lett.* **51** 39
- [3] Jarboe T.R. *et al* 1990 *Phys. Fluids B* **2** 1342
- [4] Rusbridge M.G. *et al* 1997 *Plasma Phys. Control. Fusion* **39** 683
- [5] Turner W.C. *et al* 1983 *Phys. Fluids* **26** 1965
- [6] Barnes C.W. *et al* 1990 *Phys. Fluids B* **2** 1871
- [7] Geddes C.G.R. *et al* 1998 *Phys. Plasmas* **5** 1027
- [8] Rosenbluth M.N. and Bussac M.N. 1979 *Nucl. Fusion* **19** 489
- [9] Jarboe T.R. 1994 *Plasma Phys. and Control. Fusion* **36** 945
- [10] Hagenson R.L. and Krakowski R.A. 1985 *Fusion Tech.* **8** 1606
- [11] Taylor J.B. 1974 *Phys. Rev. Lett.* **33** 1139
- [12] Low B.C. 1997 *Coronal Mass Ejections, Geophysical Monograph* 99 ed N. Crooker *et al* (Washington, DC: American Geophysical Union) p 39
- [13] McLean H.S. *et al* 2002 *Phys. Rev. Lett.* **88** 125004
- [14] Wood R.D. *et al* 2005 *Nucl. Fusion* **45** 1582
- [15] Marchiano M.M. *et al* 2005 *Proc. 15th IEEE Int. Pulsed Power Conf. (13–17 June 2005, Monterey, CA, USA)* pp 688–91  
<http://ieeexplore.ieee.org/servlet/opac?punumber=4084140>
- [16] Woodruff S. *et al* 2003 *Phys. Rev. Lett.* **90** 095001
- [17] Woodruff S. *et al* 2004 *Phys. Rev. Lett.* **93** 205002
- [18] Janos A. 1988 *Phys. Fluids* **19** 3342
- [19] Ryutov D.D. *et al* 2004 *Phys. Plasmas* **11** 4740
- [20] Duck R.C. *et al* 1997 *Plasma Phys. Control. Fusion* **39** 683
- [21] Kruskal M. and Tuck J. 1958 *Proc. R. Soc. A* **245** 222
- [22] Shafranov V. 1957 *At. Energy Aust.* **5** 38
- [23] Browning P.K. *et al* 1992 *Phys. Rev. Lett.* **68** 1718
- [24] Hsu S.C. and Bellan P.M. 2003 *Phys. Rev. Lett.* **90** 215002
- [25] Hooper E.B. *et al* 2007 *Nucl. Fusion* **47** 1064
- [26] Romero-Talamás C.A. *et al* 2006 *Phys. Plasmas* **13** 022502
- [27] Finn J.M. *et al* 1981 *Phys. Fluids* **24** 1336